Heliyon 10 (2024) e34558

Contents lists available at ScienceDirect

Heliyon

journal homepage: www.cell.com/heliyon

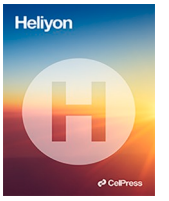

Research article

Evaluation of phytoactive contents and antibacterial activities of green synthesised cerium oxide nanoparticles using *Melastoma* sp. leaf extract as the capping agent

Nor'Aishah Hasan [a], Nurul Natasha Wazir [a], Muhamad Yusuf Samsudin [a], Muhammad Mirza Syahmi Mohd Sanizam [a], Nor Monica Ahmad [b,*], Nurul Atikah Badrol Hisham [b], Yamin Yasin [b], Nik Rozlin Nik Masdek [c]

[a] *School of Biology, Faculty of Applied Sciences, Universiti Teknologi MARA, Cawangan Negeri Sembilan, Kampus Kuala Pilah, 72000, Kuala Pilah, Malaysia*
[b] *School of Chemistry and Environment, Faculty of Applied Sciences, Universiti Teknologi MARA, Cawangan Negeri Sembilan, Kampus Kuala Pilah, 72000, Kuala Pilah, Malaysia*
[c] *School of Mechanical Engineering, College of Engineering, UniversitiTeknologi, MARA, 40450, Shah Alam, Selangor, Malaysia*

ARTICLE INFO

Keywords:
Cerium oxide nanoparticles
Melastoma sp.
Nanoparticles

ABSTRACT

Simple and green methods of developing nanoparticles (NPs) have attracted the attention of researchers. Literature on utilising leaf extract to prepare cerium oxide (CeO_2 NPs) is scarce. The present study synthesised leaf-mediated-CeO_2 NPs to produce nanopowders of controllable sizes for further applications. The study is the first to report the optimised parameters (pH 7, 5 g/150 mL concentration of the leaf extract, and 3 h of reaction time) of procuring CeO_2 NPs using *Melastoma* sp. leaf extract as the capping agent with excellent properties. The absorbance of the NPs suspension obtained in this study was recorded at approximately 252 nm with Ultraviolet–Visible (UV–Vis) Spectroscopy. Fourier Transform Infrared Spectroscopy (FTIR), Scanning Electron Microscopy (SEM), X-ray Diffraction (XRD), and Transmission Electron Microscopy (TEM) were also utilised to characterise and confirm the CeO_2 NPs prepared. The XRD spectra documented the purity of the NPs at specific diffraction patterns, while TEM revealed the spherical form of the NPs with a particle size of 16 nm. The formation of CeO_2 NPs has been confirmed from the FTIR spectra procured, which exhibited a Ce–O peak at 555 nm. Phytochemical screening test and FT-IR analysis of leaf extract revealed the existence of flavonoids, terpenoids, sugars, saponins, quinones, and glycosides. The NPs suspensions of varying concentrations (control, 50, 100, 150, 200, and 250 μg/mL) were prepared and employed for evaluations against Gram-positive and -negative bacteria. Resultantly, CeO_2 NPs demonstrated antibacterial activities against both bacteria types. The highest antibacterial activities were recorded against E. coli and *K. pneumonia* at 1.83 ± 0.137 and 1.83 ± 0.14 mm maximum inhibition zones, respectively, at 250 mg/uL of the NPs.

* Corresponding author.
E-mail address: normonica@uitm.edu.my (N.M. Ahmad).

https://doi.org/10.1016/j.heliyon.2024.e34558
Received 30 August 2023; Received in revised form 30 June 2024; Accepted 11 July 2024
Available online 14 July 2024

1. Introduction

The demand for antibacterial agents has been increasing in the past decades and could be gratified with the advancement of nanoparticles (NPs). As a consequence, the fabrication of various NPs has been studied by many researchers as ideal alternatives with high therapeutic potential [1]. The large surface-to-volume ratio of NPs enables them to work efficiently as antibacterial [2]. Nevertheless, physical characteristics, such as purity, shape, surface, and critical structures, are the parameters that influence the intrinsic activities of NPs [3]. Chemical methods are reportedly sufficient to synthesise NPs. Nonetheless, the approaches are constraining due to expensive chemicals, toxicity and agglomeration issues in their synthesising routes [4].

Consequently, biological methods of producing NPs have been explored to overcome the drawbacks of physical and chemical techniques. Furthermore, the biological synthesis route offers the advantages of green synthesis considering the various plants, including agriculture waste, ornamental, and medicinal plants. Among plant, *Melastoma* sp. is a medicinal plant that has been explored in the production of NPs via biological approaches. The Melastomataceae family includes the genus *Melastoma*, which comprises 50 to 70 species spread over India, Southeast Asia, Australia, and the Pacific Islands. The plant species has demonstrated potential as medicines. For instance, *Melastoma* sp. root juice is utilised to treat skin diseases and reduce fever and pain, while Asians have frequently utilised the leaves to treat gastrointestinal disorders [5].

Melastoma sp. possesses phytochemicals and has demonstrated high antioxidant activities. Sari et al. [6] performed phytochemical screening on *Melastoma malabathricum* (*M.malabathricum)* leaf, a *Melastoma* sp., and recorded alkaloids, flavonoids, saponin, tannin, steroids, and carbohydrates. The phytochemical constituents result in the plant being a potential reducing, stabiliser, or capping agent in the synthesis of NPs. In another study, Khan et al. [7] demonstrated the role of *M.malabathricum* leaf extract during zinc oxide (ZnO) and manganese (Mn)-doped ZnO (1 and 5 %) procurements for utilisations as antibacterial. The study reported successful production of the NPs, in which the 1 % Mn-doped ZnO documented the highest antibacterial activity against *Bacillus subtilis* at minimum inhibitory concentration.

Another part of the *M.malabathricum* plant is its flowers. Krishnaprabha and Pattabi [8] recorded that the *M.malabathricum* flowers have assisted in synthesising silver (Ag) NPs at different pH levels. Furthermore, the biosynthesised Ag NPs efficiently catalysed the degradation of methylene blue dye. In another investigation, Krishnaprabha and Pattabi [9] reported the production of gold NPs utilising varying volumes of *M.malabathricum* flower extract. Characterisation analysis performed in the investigation revealed the formation of pure crystalline spherical gold NPs particles of approximately 20–30 nm. The fruits of *M.malabathricum* have also been explored in the green procurement of Ag NPs without the employment of any chemical capping agent, which further validated the role of *M.malabathricum* in NPs preparations [10].

Numerous NPs synthesis methods have been extensively explored. For instance, Annu et al. [11] utilised pomegranate (*Punica granatum*) peel extract as the reducing and capping agents to prepare Ag NPs. The Ag NPs exhibited remarkable stability in the colloidal form and potent antimicrobial activities against Gram-positive and -negative bacteria. Furthermore, they did not demonstrate cytotoxic effects on normal cells at evaluated doses. Nevertheless, the NPs impeded A549 cell growth. In another study, Annu et al. [12] investigated the performances of plant-mediated Ag NPs prepared in sweet orange (*Citrus sinensis*) peel extract and hybrid nanocomposites developed with chitosan. The nanocomposites inhibited *Escherichia coli* and *Staphylococcus aureus* growth at 20 nm and 17.5 mm, respectively. Similarly, ZnO NPs are gaining attention due to their unique physicochemical properties, such as significant chemical and light stabilities, electrochemical coupling coefficient, and wide radiation absorbance range [13,14]. The remarkable properties of ZnO NPs were also reported by Gupta et al. [15], where bio-nanocomposites of cotton-tree flowers (*Bombax ceiba*) -mediated ZnO NPs were produced.

Titanium dioxide (TiO_2) NPs are becoming increasingly prominent due to their advantageous attributes, widespread availability, affordability, and robust chemical and thermal stabilities. The binary metal oxide possesses three polymorphs: rutile, anatase, and

Table 1
Synthesis of CeO_2 NPs by different plants.

[a]Scientific name [b]Common name	[a]Part of leaves [b]Temperature	[a]Particles size TEM (nm) [b]Crystallite size XRD (nm)	[a]Applications [b]Shape	Author
[a]*Moringa oleifera* [b]Drumstick tree	[a]Seed [b]65 °C	[a] 30 [b] 30.5	[a]Molluscicidsal activities [b]Spherical	[27]
[a]*Gloriosa superba L.* [b]Flame lily	[a]Leaves [b]80 °C	[a] 5 [b] 24	[a]Antibacterial activity [b]Spherical	[25]
[a]*Prosopis fracta* [b]Syrian mesquite	[a]Fruit [b]70 °C	[a] * [b] 22	[a]Cytotoxic activities [b]Spherical	[28]
[a]*Moringa oleifera* [b]Drumstick tree	[a]Leaves [b]80 °C	[a]17 [b]11	[a]Antimicrobial activity [b]Spherical	[26]
[a]*Salvia macrosiphon* [b]Boiss	[a]Seed [b]80 °C	[a] not perform [b] 11	[a]Photo-catalytic activities [b]Spherical	[29]
[a] *Caccinia macranthera* bNot available	[a]Leaves [b]80 °C	[a] * [b] 10.54	[a]Drug delivery [b]Spherical	[30]
[a]*Calotropis procera* [b]Giant milkweed	[a]Flower [b]85 °C	[a]21 [b]7.08	[a]Photocatalytic degradation antibacterial activity [b]Spherical	[31]
[a] *Melastoma* sp. [b] Senduduk	[a]Leaves [b]Room temperature	[a] 16.0 [b] 5.31	[a]Antibacterial activity [b]Spherical	This work

brookite, recording 3.0, 3.2, and 3.2 eV band gaps, respectively [16,17]. The material has also been employed to produce a novel nanocomposite with polyvinyl alcohol and chitosan to inhibit bacterial activities and combat the skin cancer cell line [14]. In another study, Shekhar et al. [18] noted the role of *Azadirachta Indica* leaf extract as the reducing and capping agents during TiO_2 NPs synthesis. The NPs were spherical and ranged between 10 and 20 nm after calcination at 500 °C. The research has initiated novel, simple, cost-effective, environmentally friendly, and non-toxic methods of preparing NPs.

Among promising smart materials, cerium oxide (CeO_2 NPs) is an exceptional metal oxide in the lanthanide family. The material is a preferred option for biomedical applications because of its distinct properties, such as antioxidant, anti-inflammatory, angiogenic, and antibacterial qualities [19]. The material demonstrates distinctive redox characteristics attributable to the coexistence of cerium (III) and cerium (IV) oxidation states, which results in valuable characteristics arising from its incomplete 4f-subshell. The CeO_2 NPs redox behaviour is dependent upon the capacity of the NPs to undergo reversible oxidation and reduction reactions. The multiple oxidation states of the material enable it to function as oxidising and reducing agents, contingent upon the reaction conditions [20–24].

Reports of biosynthesising CeO_2 NPs utilising plant extracts, such as seed, leaves, fruits, and flowers, are limited (see Table 1). To date, only few publications reported employing leaves extract to obtain CeO_2 NPs. Arumugam et al. [25] synthesised CeO_2 NPs with Flame lily (*Gloriosa superba* L.) leaf extract, where the effectiveness of the green NPs on Gram-positive and -negative bacteria was examined via disc diffusion method. The report documented that Gram-positive bacteria were relatively more susceptible to the NPs than their Gram-negative counterparts. Similar findings were reported by Putri et al. [26], where CeO_2 NPs were successfully synthesised with Drumstick tree (*Moringa oleifera*) leaf extract through a rapid green precipitation approach.

A green method of producing nanomaterials that are less harmful to the environment is crucial. Currently, no literature is available on green synthesising CeO_2 NPs with *Melastoma* sp. leaf extract (see Fig. 1) and the effects of the parameters employed on the formation of the NPs. Furthermore, no report has included the employment of the leaf extract as a capping agent in producing CeO_2 NPs. The available literature only describes procuring CeO_2 NPs with other plant species without reaction parameters optimisation. Inorganic NPs produce reactive oxygen species, causing disruption to the bacterial cell cycle, leading to bacterial death [32]. Nonetheless, several factors require investigation when considering to further augment the pathogenic bacteria inhibition properties of NPs, including morphology, shape, preparation method, surface roughness and energy [33,34]. The strategies should also aim to create innovative and environmentally sustainable CeO_2 NPs with tailored morphologies and reduced sizes to enhance their surface area-to-volume ratios, thereby improving their interactions with bacterial cells.

The present study attempted to synthesise CeO_2 NPs with *Melastoma* sp. to assess the potential of the bioactive compounds in the herbal plant to enhance the performance of the resultant NPs. The influences of reaction conditions (pH, extract concentration, and reaction time) on the characteristics of the NPs obtained and their performance as antibacterial agents were also examined. Furthermore, the effects of the leaf extract as stabilising and capping agents on structural properties were evaluated through ultraviolet–visible (UV–Vis), X-ray diffraction (XRD), and Fourier-transform infrared (FTIR).

The morphology and size of the NPs obtained in this study were evaluated with field emission scanning electron microscopy (FESEM) equipped with energy dispersive X-ray (EDX)-analysis (FESEM-EDX) and transmission electron microscope (TEM). The antibacterial activities of the procured NPs against Gram-negative and -positive bacteria were also examined. This study describes a straightforward, affordable, and environmentally friendly method for developing enhanced novel CeO_2 NPs utilising *Melastoma* sp. for antibacterial applications.

Fig. 1. Leaves of the *Melastoma* sp.

2. Materials and methods

2.1. Material

The Cerium (III) nitrate hexahydrate ($CeNO_3{\cdot}6H_2O$) employed in the current study was purchased from Sigma-Aldrich Corporation, Co, St Louis, Unites States of America (USA), sodium hydroxide (NaOH) was from Chemiz, Malaysia, and ethanol was from Fisher Scientific (M) Sdn Bhd, Malaysia. Gallic acid, folin-ciocalteu reagent, sodium carbonate, sulphuric acid (95–98 %), hydrochloric acid (37 %), benedict's reagent, ninhydrin reagent, glacial acetic acid, and dimethyl sulfoxide were used of analytical grade from Merck, United States.

2.2. Collection and preparation of Melastoma sp. leaf samples and extracts

The *Melastoma* sp. leaves utilised in the present study were collected from Mount Ophir (Gunung Ledang), Johor, Malaysia, at 2°22′00.0″N 102°37′00.0″E. Subsequently, the obtained leaves were authenticated at the Centre for Authentication of Herbal Raw Material (CAHRM), Forest Research Institute Malaysia (FRIM), Selangor, Malaysia.

The leaves were separated from their stalks, stems and fruits before washing them with tap water to remove dust and other foreign materials. The leaves were then left to dry under a shed for seven days in the open air. Once dried, the leaves were ground to a fine size. Subsequently, 10 g of the ground leaves was placed in a beaker containing 100 mL distilled water and boiled for 10 min. The volume of the solution procured, which had been reduced from the heating, was topped up to 100 mL prior to usage. The extract was allowed to cool before filtering through a Whatman No.1 filter paper. The supernatant was collected and kept in Schott bottles at 4 °C until further use. For total phenolic content (TPC) analysis, 20 g of dried leaves was mixed with 100 mL of methanol, filtered and the supernatant was brought to a rotary evaporator to obtain the extract before drying.

2.3. Phytochemical screening and determination of total phenolic content of Melastoma sp. leaf extracts

The procedure for the determination of TPC was followed Molole et al. [35] with brief modifications. Gallic acid was used as a standard to prepare a standard calibration curve at 0–250 μg/mL in methanol. Before the experiment, 1 mL of Folin–Ciocalteau reagent was added to 9 mL distilled water to prepare 10 % of reagent. Then, 1 mL of *Melastoma* sp., extract was added with 1 mL of diluted Folin–Ciocalteau reagent in a cuvette. The mixture was added with distilled water and 2 % Na_2CO_3 (1 mL each). A sample was left in the dark for 45 min and the absorbances of the samples were measured at 765 nm using a spectrophotometer. The TPC was expressed as mg gallic acid (GAE) per g dry extract. The present study performed a phytochemical analysis of the leaf extract according to the procedure described in a previous report [36].

2.3.1. Flavonoid assessment

The leaf extract obtained in the current study was treated with 2–3 drops of NaOH solution. The intense yellow observed indicated the presence of flavonoids, which then changed to colourless after adding some drops of sulphuric acid (H_2SO_4).

2.3.2. Terpenoid evaluation (Salkowski test)

The leaf extract (5 mL) was mixed with chloroform (2 mL) before carefully added 3 mL of concentrated H_2SO_4 to form a layer. A reddish-brown colouration between the leaf extract and H_2SO_4 layers was observed, confirming the presence of terpenoids in the extract examined.

2.3.3. Steroid assessment

A total of 1 mL of the *Melastoma* sp. extract prepared in this study was poured into a test tube and dissolved with chloroform (10 mL). Subsequently, an equal volume of concentrated H_2SO_4 was added to the test tube. The upper layer of the mixture in the test tube turned red, while the H_2SO_4 layer was yellow with green fluorescence. The observations indicated the presence of steroids in the leaf extract.

2.3.4. Reducing sugar evaluation (Benedict's test)

This study added Benedict's reagent to the previously prepared leaf filtrate at a 1:1 ratio. The mixture was then heated in a boiling water bath for 2 min. A red precipitate confirmed that the *Melastoma* sp. leaf extract evaluated contained reducing sugars.

2.3.5. Protein assessment (ninhydrin test)

A few drops of Ninhydrin reagent were incorporated into 1 mL of the leaf extract prepared in the current study before heating the solution mixture in a boiling water bath. The purple-blue observed indicated the presence of proteins.

2.3.6. Assessment for saponin (Frothing test)

In this study, the *Melastoma* sp. leaf extract prepared previously was diluted with distilled water and shaken for 15 min in a graduated cylinder. A 1 cm foam layer confirmed that saponins were present in the extract.

2.3.7. Evaluation for quinones

A total of 0.5 mL of concentrated HCl was added to 1 mL of the leaf extract prepared. Quinones were present in the *Melastoma* sp. leaf extract when a yellow precipitate was observed.

2.3.8. Assessment for glycoside

In this study, the *Melastoma* sp. leaf extract was evaluated for glucoside. First, glacial acetic acid (2 mL) was mixed with a few drops of ferric chloride. Subsequently, 5–6 drops of concentrated sulphuric acid were added to leaf extract filtrate, shaken gently, and allowed to stand. The presence of triterpenes (phytosterol) was confirmed by the golden-yellow resulting mixture observed.

2.4. Synthesising CeO_2 NPs with the Melastoma sp. leaf extracts at different parameters

The current study synthesised CeO_2 NPs following the method reported by Muthuvel et al. [31] and Janaki et al. [37] with slight modifications. First, 5.0 g of $CeNO_3{\cdot}6H_2O$ was weighed and dissolved in 100 mL of the plant extract before the mixture was stirred with a magnetic stirrer for 1 h for complete solubilisation. Subsequently, 2 M NaOH was added dropwise while mildly stirring the mixture to achieve solutions with different pHs, which were 7, 8, 9, 10, and 11. The solutions obtained were then stirred continuously for another 2 h with a magnetic stirrer.

The *Melastoma* sp. leaf extract with the pH identified as optimum was employed in determining the subsequent parameter namely ideal plant concentration and reaction time. A solution containing the optimum pH, plant concentration and reaction time obtained from the highest obsorbances measured via UV–Vis spectra was centrifuged and washed alternately with water and ethanol to remove impurities. A yellow CeO_2 NPs gel was obtained, which was then hot air oven dried at 80 °C overnight. The resultant samples were ground, sieved, and calcined at 500 °C for 2 h. Fig. 2 illustrates the CeO_2 NPs synthesis stages employed in the current study.

2.5. Characterisation of the CeO_2 NPs

The synthesised CeO_2 NPs were characterised with a doube beam UV–Vis spectrophotometer (T80+, PG Instruments) between 240 and 400 nm. The aqueous solution of CeO_2 NPs was filled in a UV-Cuvette after base line correction using blank references. The UV–Vis absorption spectra for all aqueous solution was recorded and data were plotted using Microsoft Office Excel. The surface morphology and shape of the CeO_2 NPs produced in the current study were examined with SEM equipped with EDX-analysis (A Hitachi TM3030 PLUS model) and TEM (Talos L120C). Moreover, FTIR (PerkinElmer) in the range of 4000–400 cm^{-1} was employed to analyse the CeO_2 NPs significant functional groups.

The XRD analysis of the samples obtained in the current study was conducted by employing a Rigaku diffractometer. The diffraction spectra were obtained between 20 and 80° with a monochromatic CuKα at 1.5406 Å wavelength, 2 deg/min scan speed, and

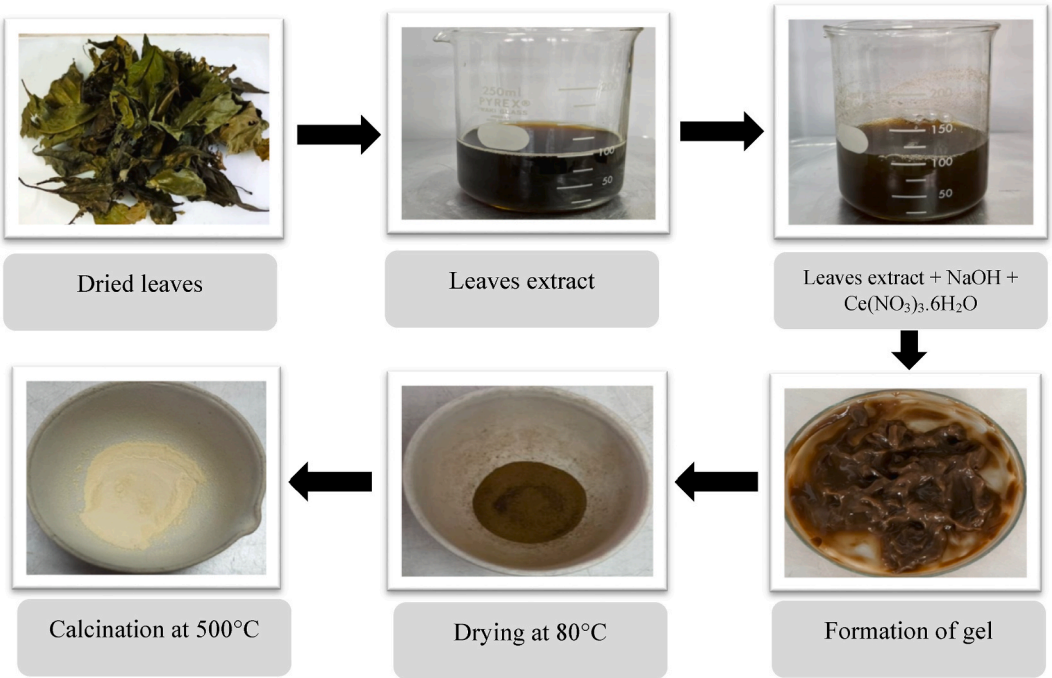

Fig. 2. Stages of green synthesis of Cerium oxide nanoparticles from Cerium nitrate precursor using the plant extract of *Melastoma* sp. as stabiliser and capping agent. (For interpretation of the references to colour in this figure legend, the reader is referred to the Web version of this article.)

0.01° step size. The standard data for HA (Card No. 9–432) and β-TCP (Card No. 009–0169) from the International Centre for Diffraction Data (ICDD) reference files were compared with the phases that were observed. Using the PDXL software, the unit cell characteristics of the samples were obtained from the XRD data.

2.6. Protocol followed for antibacterial studies

2.6.1. Bacteria strains preparation

Gram-negative bacteria, such as *Escherichia coli* (*E. coli*), *Klebsiella pneumoniae* (*K. pneumoniae*), and *Pseudomonas aeruginosa* (*P. aeruginosa*), and a Gram-positive bacteria, *Bacillus subtilis* (*B. subtilis*), were procured from the Culture Bank, Laboratory of Microbiology, Universiti Teknologi MARA Cawangan Negeri Sembilan, Kampus Kuala Pilah. The bacteria were cultured in a nutrient broth (NB) (Merck, Germany) at 37 °C for 24 h with 200 rpm agitation.

2.6.2. In-vitro susceptibility assessment (disk diffusion method)

The antibacterial activities against the selected Gram-negative foodborne pathogens of the CeO_2 NPs produced in the present study were determined through the disk diffusion susceptibility test method [38]. The bacterial strains were spread on Mueller-Hinton agar (MHA) (Merck, Germany) with sterile cotton swabs. Sterile blank antimicrobial susceptibility disks were loaded with 10 μL of varying concentrations of the prepared CeO_2 NPs. Subsequently, the disks were placed on the agar plate and incubated at 37 °C. After incubation for 24 h, the zone of inhibition was observed. A gentamicin standard disc (10 μg) served as the positive control, and 10 μL of Dimethyl sulfoxide (DMSO) was used as the negative control. Experiments were performed independently and triplicate data were analyzed using one-way variance analysis (ANOVA) followed by Tukey's post hoc test. A value of $p < 0.05$ was considered significant.

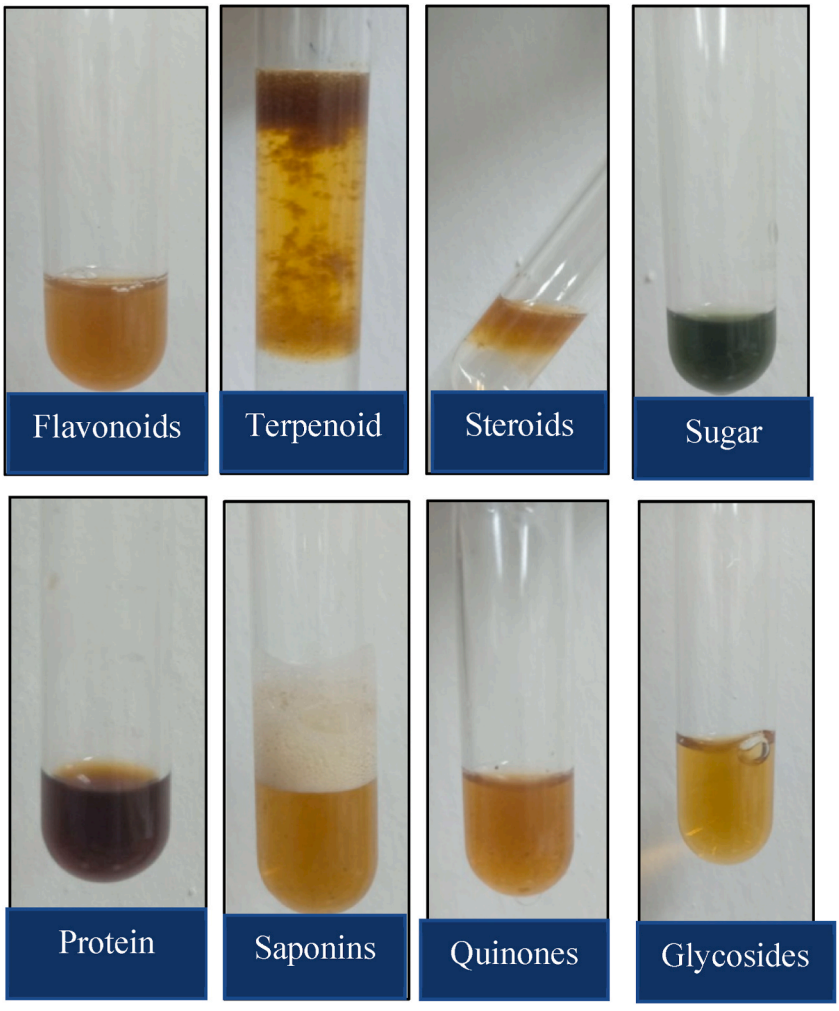

Fig. 3. Observation on the phytochemical analysis of leaves extract.

3. Results and discussion

3.1. Phytochemical screening and total phenolic content of the Melastoma sp. leaf extract

Phytochemicals, such as saponins, flavonoids, triterpenes, flavan-3-ols, anthocyanins, tannins, steroids, and phenolics have been reported to contribute to the numerous pharmacological attributes of *Melastoma* sp. The presence of flavonoids and terpenoids indicates that the plant species could be employed as remedies and natural antioxidant agents. Consequently, numerous researchers have further investigated the potential of the herb. This study conducted phytochemical screening evaluations to detect phytochemical compounds in the prepared Melastoma sp. leaf extract. Fig. 3 and Table 2 illustrate the presence of various phytochemicals from the extract, including flavonoids, terpenoids, saponins, quinones, sugar, and glycosides. The results aligned with the report by Me et al. [39], which documented flavonoids, terpenoids, and other bioactive compounds, including saponins, phenols, tannins, alkaloids, and steroids, in *M.malabathricum.* The findings also validated the utilisation of several plants from the *Melastomataceae* family by traditional folks to treat ailments such as diarrhoea, puerperal infection, dysentery, leucorrhoea, and haemorrhoids and wound healing [40, 41].

No steroid was detected in the leaf extract samples evaluated in the current study. The results contradicted the findings by Zakaria et al. [41], Simanjuntak [42], and Danladi et al. [43], who recorded the presence of steroids in the methanolic, ethanolic, and ethyl acetate extracts of the plant. According to Iloki-Assanga et al. [44], the extractability of a particular component depends on the extraction medium polarity and the solute-to-solvent ratio. In addition, TPC was assessed utilising the Folin–Ciocalteu reagent. The calibration curve ($y = 0.0054x - 0.0411$) with a correlation coefficient ($R^2 = 0.9734$) for gallic acid (0–250 μg/mL) was used to express TPC in gallic acid equivalents (GAE) per gram of dry extract. The TPC in *Melastoma* sp. leaf extract was found as 97.56 ± 12.21 mg GAE/g.

3.2. The effect of different optimisation parameters

3.2.1. Effect of pH on absorbance

Fig. 4(A) illustrates the UV–Vis absorption spectra of the CeO_2 NPs prepared at different pHs. At pHs 10 and 11, no discernible peak was identified and no significant peaks were exhibited by the precursor and leaf extract at 251 nm. Nonetheless, a peak was observed with rising absorbance when lower pH was utilised to produce the CeO_2 NPs. At pH 7, an optimum absorbance was observed at 251 nm. Consequently, *Melastoma* sp. leaf extract at pH 7 was employed as the optimised parameter for synthesising CeO_2 NPs.

Several studies have successfully produced CeO_2 NPs without pH alterations [27,28,45,46]. This study attempted to synthesise NPs at the pH of the extract, but it was too acidic, hence unfavourable for NPs procurement. The observation was supported by Butt et al. [47], where NaOH was utilised to achieve a pH 9 for manufacturing CeO_2 NPs with *Cassia glauca* petals. Likewise, Sangsefidi et al. [48] investigated the production of CeO_2 NPs with carbohydrate sugars as a capping agent. The NPs were synthesised at pH 11 by adding NaOH dropwise before the reaction was conducted in a domestic microwave oven. Accordingly, the role of pH is crucial for the development of NPs.

3.2.2. Effect of Melastoma sp. leaf extract concentration on absorbance

The second parameter assessed in the present study was the concentration of the leaf extract. Varying concentrations of the extract (5 g/50 mL, 5 g/100 mL, 5 g/150 mL, and 5 g/200 mL) [see Fig. 4(B)] were utilised during the synthesis of CeO_2 NPs, with other factors held constant. Increasing leaf extract concentration during synthesis led to agglomeration and reduced stability of the NPs obtained. Conversely, absorbance was improved with decreasing leaf extract concentration.

The most concentrated *Melastoma* sp. leaf extract (5 g/50 mL) produced no significant UV–Vis spectra peak. Accordingly, the absorbance of a less concentrated leaf extract (5 g/150 mL) was recovered as similar as 5 g/200 mL. Moreover, a too-diluted leaf extract might not be effective as a capping agent during the formation of NPs. Therefore, the 5 g/150 mL leaf extract was chosen as the optimum parameter for the subsequent experiments.

3.2.3. Effect of reaction time on absorbance

The effects of reaction time on the CeO_2 NPs produced were determined by monitoring the reaction of the aqueous plant extract and

Table 2
The phytochemical analysis results of the *Melastoma* sp. leaf extract.

Phytochemical	Test	Finding	Observation
Flavonoids		+++	An intense yellow that turned colourless with the addition of a few drops of dilute acid
Terpenoids	Salkowski	+++	Reddish-brown
Steroids		–	A red lower chloroform layer
Sugars	Benedict	+	A red precipitate
Proteins	Ninhydrin	–	Purple blue
Saponins	Frothing	+++	Frothing
Quinones	HCl	+++	Yellow
Glycosides		+++	Yellow

Note: + denotes presence, ++ indicates sharply present, and - represents absence.

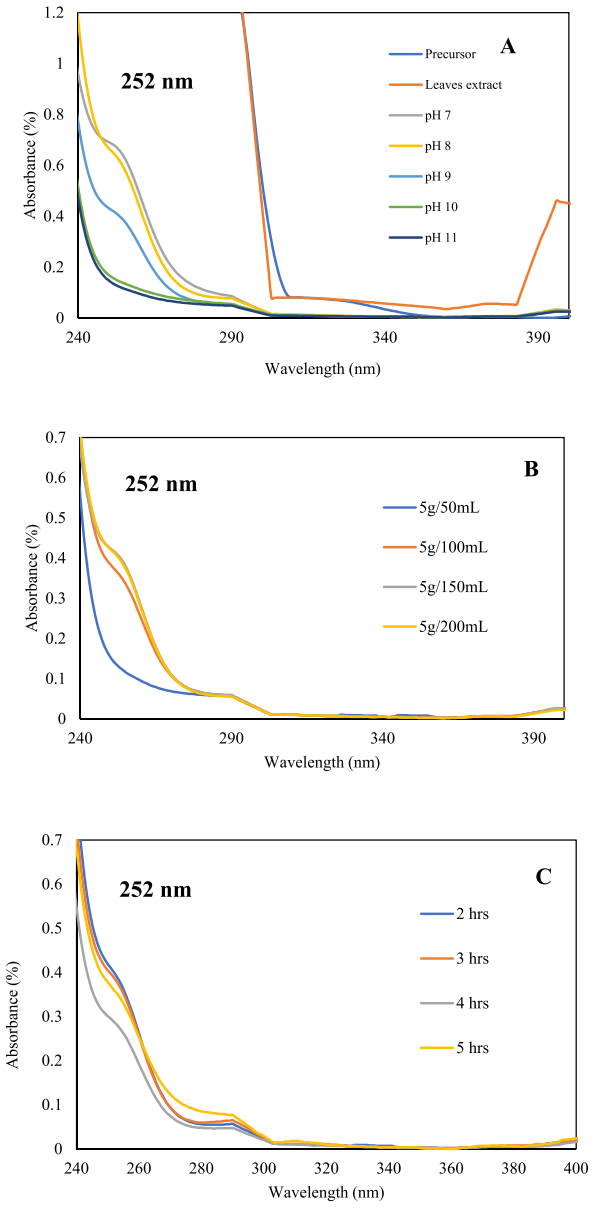

Fig. 4. UV–Vis spectra for optimisation of A) pH, extract concentrations and reaction time in the formation of CeO_2-NPs.

precursor solution under agitation with a magnetic stirrer for 2, 3, 4, and 5 h. The gradual decrease in the absorbance spectrum at 252 nm was observed when a longer reaction time was applied, as illustrated in Fig. 4(C). Nevertheless, maximum absorbances were observed at 2 and 3 h of reaction time.

Increasing the reaction time produced was avoided to prevent unwanted changes to the CeO_2 NPs. Dutta et al. [49] reported the synthesis of CeO_2 NPs at pH 7.5, in which the pH of the NPs suspension decreased gradually from 8.5 to 7.5 after 48 h, possibly due to an oxidising agent reaction from the NaOH. Consequently, the present study synthesised CeO_2 NPs under optimised conditions of 5 g/150 mL *Melastoma* sp. leaf extract at pH 7 and 3 h of reaction time while stirring. The resultant CeO_2 NPs documented a sharp peak at 252 nm.

3.3. Characterisation

3.3.1. The UV–Vis spectra analysis

The present study examined the effects of pH, the concentration of the *Melastoma* sp. leaf extract, and reaction time on the formation of CeO_2 NPs. Interestingly, the biological source and the synthesis conditions (temperature, pH, and period) altered the particle size, shape, morphology, and distribution of the resultant NPs, which were also documented by Maleki et al. [50]. The NPs of a specific

size, shape, and enhanced stability could be developed at a particular pH, considering that altering pH would result in the aggregation of the NPs to form larger NPs or initiate nucleation, forming new NPs [51].

The NPs suspension was colourless; however, its UV–Vis absorption spectrum exhibited a distinct peak at approximately 251 nm. The finding was almost identical to the observations reported by Dutta et al. [49], where a peak at 270 nm was observed when aloe vera leaf extract (capping agent) and NaOH were employed to prepare CeO_2 NPs.

3.3.2. The XRD evaluation

The XRD analysis is a non-destructive analytical method that provides information on the different phases, structures, and crystal orientations of substances. The diffraction patterns recorded at the 2 theta angles, 28.60, 33.05, 47.58, 56.38, 59.33, 69.57, 77.00, 79.02, and 88.58, corresponding to the lattice planes (111), (200), (220), (311), (222), (400), (331), and (420), respectively. The spectra documented in this study were similar to the report by Sebastiammal et al. [52], in which the CeO_2 NPs were synthesised with fruit extract.

Fig. 5 illustrates the XRD patterns obtained, which were then matched to the ICDD (International Centre for Diffraction Data) Card No. 01-083-9465. No additional peaks in the results indicated that the plant extract was an effective stabilising agent. Moreover, the data proved the cubic crystal structure of the CeO_2 NPs procured. Equation (1) was employed to calculate the crystalline size of NPs based on Debye Scherrer's formula.

$$\text{Crystalline size} = k\lambda / \beta \cos\theta \quad \text{(Eq.1)}$$

where $k = 0.9$ represents the Scherrer constant, the X-ray wavelength is $\lambda = 0.154$ nm, and the β denotes the full-width half maximum [53]. The particle size of the CeO_2 NPs was 5.31 nm. The relatively smaller size might be due to the superior capping agent of the leaf extract in controlling the growth of the NPs. The particle size of the NPs produced in the present study was smaller than those reported by Iqbal et al. [45] that synthesised CeO_2 NPs in *Coriandrum sativum* (11.36 nm).

3.3.3. The FTIR analysis

The FTIR spectra analysis in this study was performed with potassium bromide (KBr) pellets to visualise the functional groups of CeO_2 NPs at wavelengths from 450 to 4000 cm^{-1} as demonstrated in Fig. 6. A Ce–O stretching vibration peak was observed at 535 cm^{-1}, validating the formation of CeO_2. Similar results were reported by Parimi et al., who noted that the Ce–O stretching frequency was observed at approximately 500 cm^{-1} [54]. The same pattern was observed by Umar et al. [55] during the chemical synthesis of CeO_2 NPs in hexamethylenetetramine as the capping agent. A strong peak at 555 cm^{-1} was observed due to Ce–O stretching vibrational modes, which confirmed the formation of Ce–O bonds in the NPs.

Another significant peak was observed at 1116 cm^{-1} that corresponded to Ce–*O*–Ce vibration, which was also recorded by Iqbal et al. [45]. The peak obtained around 841 cm^{-1} resulted from C–C bending produced by Ce–O stretching vibrations in the CeO_2, as agreed by *Rajesh* et al. [56]. A broad peak at 3423 cm^{-1} specified the O–H vibration of the water groups present [46]. The water molecules might be incorporated during the preparation of the CeO_2 NPs [57]. Moreover, the large charge and low basicity of the Ce^{4+} might promote hydration [58]. The nature of the compounds contained in the plant extract, such as flavonoids, polyphenols, and phenolic acids, also offers another possible explanation [59].

The alkene (C═C), C–N, polyphenol (C═O), and aromatic ring (C═C) stretchings and bending and vibrations of the alkane (C–H) groups were observed at 1565, 1364, and 1116 cm^{-1}, as per the findings by Chandrasekaran et al. [60]. Furthermore, the results were well supported by the peak documented at 1634 cm^{-1}, which indicated the C═C stretching from the cyclic alkene. The peak also revealed that the functional groups from the chemical compounds in the leaf extract have remained on the surfaces of the CeO_2 NPs.

3.3.4. The TEM assessment

The TEM is conducted to confirm the size, shape, and dispersion of assessed particles [61]. The CeO_2 NPs manufactured in the

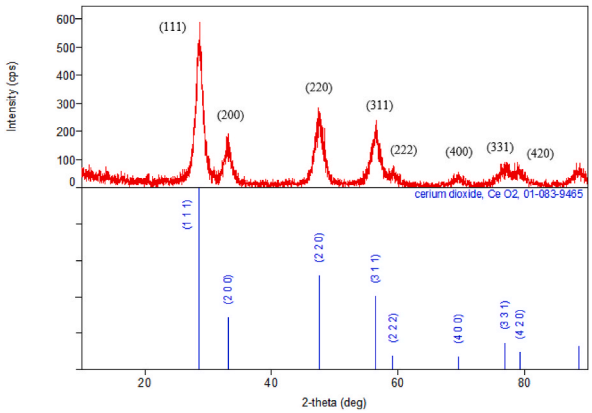

Fig. 5. XRD pattern of CeO_2 NPs.

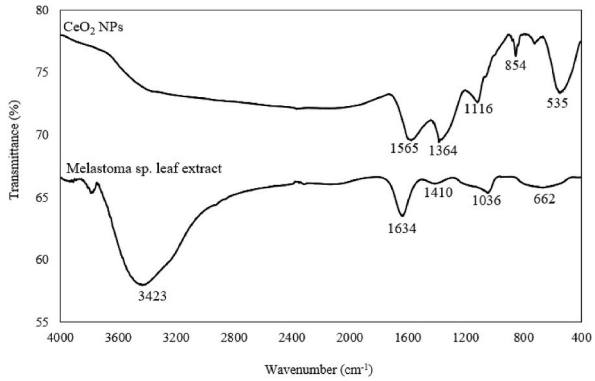

Fig. 6. FTIR spectra of a) CeO_2 NPs and b) *Melastoma* sp. leaf extract.

present study were very small and dense black spheres as exhibited in Fig. 7(A). Morphology assessment of CeO_2 NPs in leaf extract yielded clusters with aggregation. In the present study, the agglomeration of the NPs is primarily attributed to the accumulation of two or more reducing agents attached to preformed nuclei surfaces [62]. This might be due to the phytochemical compound-rich plant extracts were utilised as the reducing and capping agents in synthesising NPs [63]. The morphology of the NPs was similar to the CeO_2 NPs synthesised in rutin via a one-pot synthesis method reported by Sathiyaseelan et al. [64]. The TEM histogram, demonstrated in Fig. 7(B), revealed that the NPs obtained in the current study possessed an average particle size of 16.0 nm.

The particle size of the CeO_2 NPs manufactured in the present study was calculated from the TEM image with Image-J software in 100 random particles. Subsequently, the data were employed to plot the size histogram. The particle size distribution histogram was similar to the results recorded by Bilal et al. (26.62 nm) [65], in which the synthesis of nickel ferrite NPs utilised green cabbage and Utara et al. [66], who obtained 11.7 nm CeO_2 NPs post-calcination at 300 °C for 3 h.

3.3.5. The FESEM-EDX assessment

The SEM enables the visualisation of the morphologies of materials assessed and it has also been employed to determine the structures and morphologies of NPs [67]. Fig. 8(A) illustrates the SEM micrograph images of the surface morphology of the CeO_2 NPs synthesised with *Melastoma* sp. leaf extract prepared in this study. The micrograph demonstrates the agglomeration and irregular shapes of the NPs particles. Similarly, Butt et al. [47] observed agglomerations while synthesising CeO_2 NPs with *Cassia glauca* petals. The study suggested that agglomeration is common on tiny particles.

Agglomeration typically occurs due to the tendency of NPs to reduce their exposed surface area to lower surface energy. Consequently, smaller particle sizes would result in a stronger agglomeration [47]. The EDX spectrum of the CeO_2 NPs procured in the present study [see Fig. 8(B)] demonstrated high percentages of oxygen and Ce. Small amounts of other elements, including carbon, phosphorus, sulphur, chlorine, potassium and calcium were also documented in the NPs. Nonetheless, a substantial amount of sodium was detected due to utilising NaOH as a precipitation agent during synthesis.

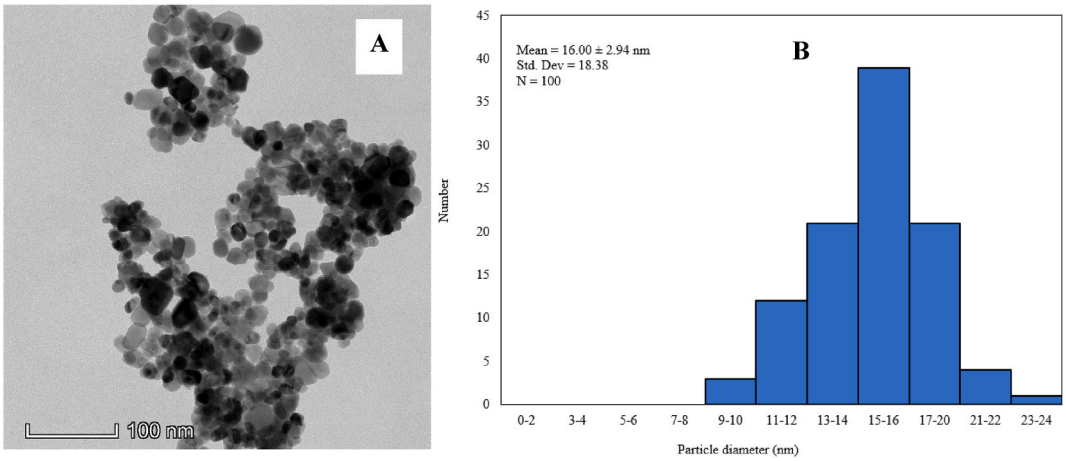

Fig. 7. TEM images of A) CeO_2 NPs and B) size distribution histograms obtained from TEM images.

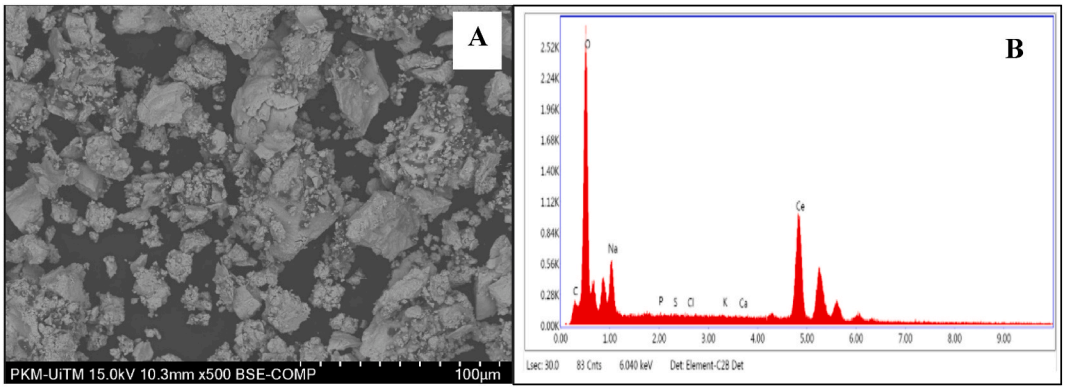

Fig. 8. FESEM images (A) and EDX analysis (B) of CeO_2 NPs.

4. Antibacterial activity of the CeO_2 NPs against pathogens

In this study, the antimicrobial potential of the CeO_2 NPs produced against three species of Gram-negative (*Escherichia coli*, *Klebsiella pneumonia*, *Pseudomonas aeruginosa*) and one Gram-positive bacteria (*Bacillus subtilis*) was examined through the agar well diffusion method. The clear zones observed around the CeO_2 NPs disks during the disk diffusion assessment confirmed the antibacterial activities of the NPs (see Fig. 9). Similar to the findings by Barker et al. [68], the CeO_2 NPs produced in this study inhibited the growths of the Gram-negative foodborne pathogens. Nevertheless, the CeO_2 NPs (250 µg/mL) were ineffective against *Pseudomonas aeruginosa* (*P. aeruginosa*).

The inhibition zones observed around the NP disks were between the 1.4 ± 0.08–1.83 ± 0.14 range (see Table 3). At 250 µg/mL, the CeO_2 NPs recorded a maximum inhibition zone of 1.83 ± 0.137 against *Escherichia coli*, 1.83 ± 0.14 mm against *Klebsiella pneumonia*, and 15.4 ± 0.04 mm against *Bacillus subtilis*. The antibacterial efficacy of the CeO_2 NPs against the pathogens assessed was considerable and statistically significant, except towards *P. aeruginosa*, which was the most resistant against the CeO_2 NPs (see Table 3). Moreover, the CeO_2 NPs were more effective and enabled faster adsorption of pathogens than bulk NPs due to their small size.

Numerous mechanisms of the antibacterial activities NPs metal oxide, particularly CeO_2 NPs, have been reported. Zhang et al. have detailed the antibacterial mechanisms of CeO_2 NPs and the variables affecting the mechanisms [69]. The CeO_2 NPs either directly interact with pathogens or produce secondary toxic chemicals that harm or kill cells. According to a study, reactive oxygen species (ROS) formation has also been linked to the effective bactericidal action of CeO_2 NPs [70]. NPs are small particles with large specific surface areas. Increasing NPs concentration improves the contact areas between the nanoparticles and microorganisms, leading to more thorough reactions and enhanced bactericidal impact. Furthermore, elevated NPs concentrations improve charge carriers and ROS generation. ROS surplus produced by bacteria could induce DNA damage [71,72].

Many studies have highlighted the superior antibacterial properties of CeO_2 NPs against Gram-positive and Gram-negative bacteria, as reviewed by Farias et al. [73]. In addition, the antibacterial strategies and mechanisms of CeO_2 NPs have been extensively reported in the literature [69]. In their review, the authors reported the detailed mechanisms which involve several key steps.

i. Adsorption of NPs onto the surface of cell membrane: Gram-positive and Gram-negative bacteria are negatively charged, enabling the positively charged nano-sized CeO_2 NPs to rapidly adsorb onto microorganisms through electrostatic attraction.
ii. Antibacterial activity by induced cellular toxicity and oxidative stress: Upon the attachment of the NPs on the cell membranes, reactive oxygen species (ROS) will be released from the surface of CeO_2 NPs leading to severe damage to microorganisms. ROS

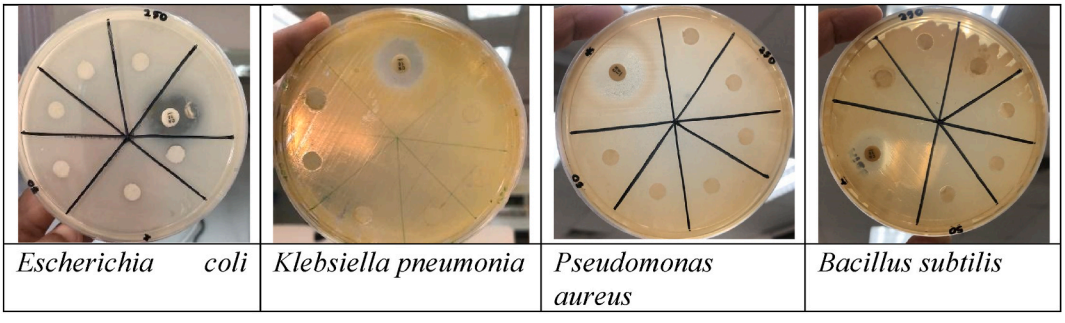

Fig. 9. Antibacterial activities of CeO_2 NPs against bacterial pathogens using a disk diffusion assay (50, 100, 150, 200, 250 µg/mL of CeO_2 NPs; 10 µg/mL gentamicin standard drug).

Table 3
Antibacterial activity of CeO_2 NPs against bacteria pathogens.

Bacteria pathogen	Concentration of CeO_2-NPs (μg/mL)					Gentamycin (μg/mL)
	50	100	150	200	250	10
Escherichia coli	1.46 ± 0.08*	1.52 + 0.02*	1.56 + 0.10*	1.66 ± 0.14*	1.83 ± 0.137*	2.06 ± 0.05
Klebsiella pneumonia	NIZ	NIZ	1.5 ± 0.05*	1.76 ± 0.23*	1.83 ± 0.14*	2.33 ± 0.14
Pseudomonas aeruginosa	NIZ	NIZ	NIZ	NIZ	NIZ	2.57 ± 0.10
Bacillus subtilis	1.4 ± 0.05*	NIZ	1.46 ± 0.05*	NIZ	1.54 ± 0.04*	2.73 ± 0.05

NIZ- No inhibition zone. (All data represent mean ± standard deviation of three replicates and all comparisons are made with gentamicin as the standard drug. *$p < 0.05$. NS-no significant).

are known to induce oxidative stress, which damages DNA, alter cell membranes permeability, and causing inhibition of translation and protein synthesis.

iii. Interruption of modulation of signal transduction pathways: CeO_2 NPs may connect with mesosomes after adhering to bacterial membranes, interfering with the nutrition transport by obstructing cellular respiration, DNA replication, and cell division [25]. The proteins on bacterial membranes contain thiol groups (–SH) which react with the ions released from NPs [74] making the proteins extrude through the cell membrane and disrupt their nutrient transport functions. The interaction between proteins and NPs inhibits phosphorylation of proteins and inhibits their enzymatic activity which results in cell death. Furthermore, the asymmetrical forms or rough surfaces of NPs containing sharp edges and corners may physically damage the bacteria.

The Gram-negative bacteria evaluated in this study were more susceptible to the CeO_2 NPs produced than the Gram-positive bacteria. The differing structure and compactness of the cell walls of the pathogens played a significant role in the diverse ways the CeO_2 NPs operate against them. Gram-positive bacteria typically possess thicker and waxier cell walls than their Gram-negative counterparts, thus more resistant to the CeO_2 NPs antibacterial effects [75]. The overall data demonstrated that the standard drug gentamicin produced a higher inhibition zone against all the bacteria assessed.

In this study, the antimicrobial potential of CeO_2 NPs was evaluated against three species of Gram-negative bacteria (*Escherichia coli, Klebsiella pneumoniae, Pseudomonas aeruginosa*) and one Gram-positive bacterium (*Bacillus subtilis*). Future research of our work should consider assessing the antibacterial activity of these NPs against more bacteria such as *Salmonella enterica typhi*, *Shigella* sp., and *Mycobacterium* sp. The superior ability of copper, Zn, nickel, and Ag NPs to inhibit and kill *Salmonella enterica typhi* was reported by Kapadia et al., [76]. The results of the antimicrobial evaluation showed Ag NPs, either used alone or in combination, had potent antibacterial activity against all pathogenic *Salmonella* sp. Furthermore, Vidyasagar et al. [77], reported the biological activity of Ag NPs made from *Clerodendrum serratum* plant shows excellent antimicrobial properties against *Mycobacterium* sp. The NPs exhibited maximum inhibitory activity against Tubercular and Non-Tuberculous Mycobacterium species i.e., *Mycobacterium smegmatis, Mycobacterium fortuitum and Mycobacterium marinum.* Also, Ayodele et al. [78], reported chitosan NPs containing Cu(II) and Ni(II) ions exhibited strong antibacterial activity against *Shigella* and *Salmonella* sp.

5. Conclusion

The present study successfully synthesised CeO_2 NPs utilising *Melastoma* sp. leaf extract as the capping agent. Assessments with ultraviolet–visible (UV–Vis) spectroscopy established pH 7, 0.1 g/mL plant extract concentration, and 3 h reaction time as the optimal conditions for producing CeO_2 NPs with *Melastoma* sp. leaf extract. Characterisation evaluations revealed that the CeO_2 NPs obtained were under 20 nm. The XRD results confirmed the purity of the procured NPs, which demonstrated no unwanted peaks, and the spherical morphology of the NPs were recorded with TEM and FESEM. The FTIR spectra also demonstrated the presence of Ce–O bonding and residual functional groups from the phytochemical compounds of the leaf extract. Moreover, antibacterial assessments indicated the significant CeO_2 NPs antimicrobial activities against Gram-positive (*B. subtilis*) and -negative (*E. coli* and *K. pneumonia*) bacteria, suggesting its potential as a novel antimicrobial agent for combating bacterial infections, including those caused by multidrug-resistant pathogens.

Funding

The authors gratefully acknowledge the financial support provided by Geran Penyelidikan Sanjung Sarjana (GSS) , from Universiti Teknologi MARA, Malaysia [600-RMC/GSS (030/2022)]

CRediT authorship contribution statement

Nor'Aishah Hasan: Writing – review & editing, Supervision. **Nurul Natasha Wazir:** Methodology. **Muhamad Yusuf Samsudin:** Methodology. **Muhammad Mirza Syahmi Mohd Sanizam:** Methodology. **Nor Monica Ahmad:** Writing – review & editing, Writing – original draft, Supervision, Formal analysis, Conceptualization. **Nurul Atikah Badrol Hisham:** Methodology. **Yamin Yasin:** Writing – review & editing. **Nik Rozlin Nik Masdek:** Writing – review & editing.

Declaration of competing interest

The authors declare that they have no known competing financial interests or personal relationships that could have appeared to influence the work reported in this paper.

Acknowledgement

The authors would also like to extend their gratitude to the Faculty of Applied Science UiTM Shah Alam and the Centre for Research and Instrumentation Management (CRIM) for their analytical services. Furthermore, the authors thank Johor National Park for allowing plant sample collection.

References

[1] S. Singla, A. Jana, R. Thakur, C. Kumari, S. Goyal, J. Pradhan, Green synthesis of silver nanoparticles using Oxalis griffithii extract and assessing their antimicrobial activity, OpenNano 7 (100047) (2022) 1–11, https://doi.org/10.1016/j.onano.2022.100047.
[2] S. Rajagopalachar, J. Pattar, S. Mulla, Synthesis and characterization of plate like high surface area MgO nanoparticles for their antibacterial activity against Bacillus cereus (MTCC 430) and Pseudomonas aeruginosa (MTCC 424) bacterias, Inorg. Chem. Commun. 144 (109907) (2022) 1–9, https://doi.org/10.1016/j.inoche.2022.109907.
[3] A. Selmani, D. Kovacevi, K. Bohinc, Nanoparticles : from synthesis to applications and beyond, Adv. Colloid Interface Sci. 303 (102640) (2022) 1–12, https://doi.org/10.1016/j.cis.2022.102640.
[4] D. Ayodhya, A. Ambala, G. Balraj, M. Pradeep, P. Shyam, Green synthesis of CeO2 NPs using Manilkara zapota fruit peel extract for photocatalytic treatment of pollutants , antimicrobial , and antidiabetic activities, Results Chem 4 (100441) (2022) 1–16, https://doi.org/10.1016/j.rechem.2022.100441.
[5] V.L. Nozlena Abdul Samad, Nik Nur Syazni Nik Mohamed Kamal, Noorfatimah Yahaya, Mohd Yusmaidie Bin Aziz, Nur Nadhirah Mohamad Zain, Nor Adlin Md Yusoff, Ethnobotanical, phytochemical, and pharmacological aspects of Melastoma sp, Malaysian J. Med. Heal. Sci. 14 (2018) 153–163.
[6] N.M. Sari, H. Kuspradini, R. Amirta, I.W. Kusuma, Antioxidant activity of an invasive plant, Melastoma malabathricum and its potential as herbal tea product, IOP Conf. Ser. Earth Environ. Sci. 144 (1) (2018) 1–7, https://doi.org/10.1088/1755-1315/144/1/012029.
[7] M.M. Khan, M.H. Harunsani, A.L. Tan, M. Hojamberdiev, S. Azamay, N. Ahmad, Antibacterial activities of zinc oxide and Mn-doped zinc oxide synthesized using Melastoma malabathricum (L.) leaf extract, Bioprocess Biosyst. Eng. 43 (8) (2020) 1499–1508, https://doi.org/10.1007/s00449-020-02343-3.
[8] M. Krishnaprabha, M. Pattabi, Biogenic synthesis of fluorescent silver nanoparticles using Melastoma Malabathricum flower extract, AIP Conf. Proc. 1832 (2016) 1–4, https://doi.org/10.1063/1.4980249.
[9] M.P. Krishnaprabha M, Melastoma malabathricum flower extract mediated rapid synthesis of spherical gold nanoparticles, Mater. Today Proc. 9 (2019) 133–141, https://doi.org/10.1016/j.matpr.2019.02.146.
[10] S.I. Salprima Yudha S, Aswin Falahudin, Meka Saima Perdani, Irfan Gustian, Melastoma malabathricum fruit extract-mediated synthesis of silver nanoparticles with sensing ability for high concentrations of mercury (II) nitrate, J. Pure Appl. Chem. Res. 6 (3) (2017) 261–267, https://doi.org/10.21776/ub.jpacr.2017.006.03.353.
[11] S. Ahmed Annu, G. Kaur, P. Sharma, S. Singh, S. Ikram, Evaluation of the antioxidant, antibacterial and anticancer (lung cancer cell line A549) activity of: punica granatum mediated silver nanoparticles, Toxicol. Res. 7 (5) (2018) 923–930, https://doi.org/10.1039/c8tx00103k.
[12] S. Ahmed Annu, R.K. Nirala, R. Kumar, S. Ikram, Green synthesis of chitosan/nanosilver hybrid bionanocomposites with promising antimicrobial, antioxidant and anticervical cancer activity, Polym. Polym. Compos. 29 (2021) S199–S210, https://doi.org/10.1177/0967391121993977.
[13] Z. Jiang, et al., Research progresses in preparation methods and applications of zinc oxide nanoparticles, J. Alloys Compd. 956 (2023) 1–27, https://doi.org/10.1016/j.jallcom.2023.170316.
[14] Annu, Z.I. Bhat, K. Imtiyaz, M.M.A. Rizvi, S. Ikram, D.K. Shin, Comparative study of ZnO-and-TiO2-Nanoparticles- functionalized polyvinyl alcohol/chitosan bionanocomposites for multifunctional biomedical applications, Polymers (2023) 1–19.
[15] M. Gupta, J. Sheikh, Annu, A. Singh, An eco-friendly route to develop cellulose-based multifunctional finished linen fabric using ZnO NPs and CS network, J. Ind. Eng. Chem. 97 (2021) 383–389, https://doi.org/10.1016/j.jiec.2021.02.023.
[16] M.A. Aashi Singh, Santosh Singh, Green chemistry based for the synthesis of titanium oxide nanoparticles using extracts of Azadirachta indica, Int. J. Innov. Sci. Res. Technol. 7 (2) (2022) 1007–1011, https://doi.org/10.1016/j.clet.2023.100607.
[17] B. Blessymol, P. Yasotha, V. Kalaiselvi, S. Gopi, An antioxidant study of titanium dioxide (TIO2) nanoparticles against mace of nutmeg in myristica fragrans houtt , rhizomes of curcuma longa linn and kaempferia galanga extracts, Results Chem 7 (2024) 1–11, https://doi.org/10.1016/j.rechem.2023.101291.
[18] S. Shekhar, S. Singh, N. Gandhi, S. Gautam, B. Sharma, Green chemistry based benign approach for the synthesis of titanium oxide nanoparticles using extracts of Azadirachta Indica, Clean. Eng. Technol. 13 (2023) 1–4, https://doi.org/10.1016/j.clet.2023.100607.
[19] H. Nosrati, M. Heydari, M. Khodaei, Cerium oxide nanoparticles: synthesis methods and applications in wound healing, Mater. Today Bio 23 (2023) 1–25, https://doi.org/10.1016/j.mtbio.2023.100823.
[20] S. Muduli, T. Ranjan Sahoo, Green synthesis and characterization of CeO2 and Ni-doped CeO2 nanoparticles and its dielectric properties, Mater. Today Proc. 74 (2023) 697–702, https://doi.org/10.1016/j.matpr.2022.10.278.
[21] V. Seminko, et al., Mechanism and dynamics of fast redox cycling in cerium oxide nanoparticles at high oxidant concentration, J. Phys. Chem. C 125 (2021) 4743–4749, https://doi.org/10.1021/acs.jpcc.1c00382.
[22] M.S. Lord, J.F. Berret, S. Singh, A. Vinu, A.S. Karakoti, Redox active cerium oxide nanoparticles: current status and burning issues, Small 17 (51) (2021) 2024, https://doi.org/10.1002/smll.202102342.
[23] M. Nyoka, Y.E. Choonara, P. Kumar, P.P.D. Kondiah, V. Pillay, Synthesis of cerium oxide nanoparticles using various methods: implications for biomedical applications, Nanomaterials 10 (1–22) (2020), https://doi.org/10.3390/nano10020242.
[24] Annu, A. Ali, R. Gadkari, J.N. Sheikh, S. Ahmed, Phytomediated synthesis of cerium oxide nanoparticles and their applications, Nanomater. Plant Potential (2019) 261–284, https://doi.org/10.1007/978-3-030-05569-1_10.
[25] A. Arumugam, C. Karthikeyan, A.S. Haja Hameed, K. Gopinath, S. Gowri, V. Karthika, Synthesis of cerium oxide nanoparticles using Gloriosa superba L. leaf extract and their structural, optical and antibacterial properties, Mater. Sci. Eng. C 49 (2015) 408–415, https://doi.org/10.1016/j.msec.2015.01.042.
[26] G. Eka Putri, Y. Rilda, S. Syukri, A. Labanni, S. Arief, Highly antimicrobial activity of cerium oxide nanoparticles synthesized using Moringa oleifera leaf extract by a rapid green precipitation method, J. Mater. Res. Technol. 15 (2021) 2355–2364, https://doi.org/10.1016/j.jmrt.2021.09.075.
[27] A.M. Ibrahim, F. Mohamed, S. Al-Quraishy, A.A.S. Abdel-Baki, H. Abdel-Tawab, Green synthesis of Cerium oxide/Moringa oleifera seed extract nano-composite and its molluscicidsal activities against biomophalaria alexanderina, J. King Saud Univ. Sci. 33 (101368) (2021) 1–9, https://doi.org/10.1016/j.jksus.2021.101368.
[28] E. Nazaripour, et al., Biosynthesis of lead oxide and cerium oxide nanoparticles and their cytotoxic activities against colon cancer cell line, Inorg. Chem. Commun. 131 (108800) (2021) 1–8, https://doi.org/10.1016/j.inoche.2021.108800.
[29] B. Elahi, M. Mirzaee, M. Darroudi, R. Kazemi Oskuee, K. Sadri, M.S. Amiri, Preparation of cerium oxide nanoparticles in Salvia Macrosiphon Boiss seeds extract and investigation of their photo-catalytic activities, Ceram. Int. 45 (4) (2019) 4790–4797, https://doi.org/10.1016/j.ceramint.2018.11.173.
[30] Z. Foroutan, et al., Plant-based synthesis of cerium oxide nanoparticles as a drug delivery system in improving the anticancer effects of free temozolomide in glioblastoma (U87) cells, Ceram. Int. (2022) 1–33, https://doi.org/10.1016/j.ceramint.2022.06.322.

[31] A. Muthuvel, M. Jothibas, V. Mohana, C. Manoharan, Green synthesis of cerium oxide nanoparticles using Calotropis procera flower extract and their photocatalytic degradation and antibacterial activity, Inorg. Chem. Commun. 119 (108086) (2020) 1–7, https://doi.org/10.1016/j.inoche.2020.108086.
[32] L. Zhou, et al., Antibiotics-free nanomaterials against bacterial keratitis: eliminating infections with reactive oxygen species (ROS), Chem. Eng. J. 482 (2024) 1–22, https://doi.org/10.1016/j.cej.2024.148978.
[33] D.U. Kapoor, R.J. Patel, M. Gaur, S. Parikh, B.G. Prajapati, Metallic and metal oxide nanoparticles in treating Pseudomonas aeruginosa infections, J. Drug Deliv. Sci. Technol. 91 (2024) 1–17, https://doi.org/10.1016/j.jddst.2023.105290.
[34] L. Wang, C. Hu, L. Shao, The antimicrobial activity of nanoparticles: present situation and prospects for the future, Int. J. Nanomedicine 12 (2017) 1227–1249, https://doi.org/10.2147/IJN.S121956.
[35] G.J. Molole, A. Gure, N. Abdissa, Determination of total phenolic content and antioxidant activity of Commiphora mollis (Oliv.) Engl. resin, BMC Chem. 16 (1) (2022) 1–11, https://doi.org/10.1186/s13065-022-00841-x.
[36] S. Khalid, A. Shahzad, N. Basharat, M. Abubakar, P. Anwar, Phytochemical screening and analysis of selected medicinal plants in Gujrat, Phytochem. Biochem. 2 (1) (2018) 2–3.
[37] N.J. Selvaraj Janaki, D.S. Ivan Jebakumar, P. Sumithraj Premkumar, Studies on the physical properties of green synthesized cerium oxide nanoparticles using Melia dubia leaf extract, Mater. Today Proc. 58 (3) (2022) 850–854, https://doi.org/10.1016/j.matpr.2021.10.035.
[38] Bauer, Antibiotic susceptibility testing by a standardized single disk method. Microbiol. Centen. Perspect., ASM Press, Wash. DC USA, 1966, pp. 40–45, 1946.
[39] M. Ropisah, et al., Phytochemical analysis and biological activities of Melastoma malabathricum and Dissochaeta gracilis, ASM Sci. J. 13 (6) (2020) 1–6.
[40] A.J.S. J, J. James, J. Thomas, P. Jayaraj, R. Varatharajan, M. Muthappan, Antibacterial and wound healing activities of Melastoma Malabathricum Linn, Afr. J. Infect. Dis. 2 (2) (2008) 68–73.
[41] Z.A. Zakaria, et al., Gastroprotective activity of chloroform extract of Muntingia calabura and Melastoma malabathricum leaves, Pharm. Biol. 54 (5) (2016) 812–826, https://doi.org/10.3109/13880209.2015.1085580.
[42] M. Simanjuntak, Ekstraksi Dan Fraksinasi Komponen Ekstrak Daun Tumbuhan Senduduk (Melastoma malabathricum. L) Serta Pengujian Efek Sediaan Krim Terhadap Penyembuhan Luka Bakar, 2008 14472.
[43] S. Danladi, et al., Phytochemical screening, total phenolic and total flavonoid content, and antioxidant activity of different parts of Melastoma malabathricum, J. Teknol. 77 (2) (2015) 63–68, https://doi.org/10.11113/jt.v77.5988.
[44] S.B. Iloki-Assanga, et al., Solvent effects on phytochemical constituent profiles and antioxidant activities, using four different extraction formulations for analysis of Bucida buceras L. and Phoradendron californicum Complementary and Alternative Medicine, BMC Res. Notes 8 (1) (2015) 1–14, https://doi.org/10.1186/s13104-015-1388-1.
[45] A. Iqbal, et al., Biogenic synthesis of CeO2 nanoparticles and its potential application as an efficient photocatalyst for the degradation of toxic amido black dye, Environ. Nanotechnology, Monit. Manag. 16 (100505) (2021) 1–16, https://doi.org/10.1016/j.enmm.2021.100505.
[46] G. Zhan, J. Huang, M. Du, I. Abdul-Rauf, Y. Ma, Q. Li, Green synthesis of Au-Pd bimetallic nanoparticles: single-step bioreduction method with plant extract, Mater. Lett. 65 (2011) 2989–2991, https://doi.org/10.1016/j.matlet.2011.06.079.
[47] A. Butt, J.S. Ali, A. Sajjad, S. Naz, M. Zia, Biogenic synthesis of cerium oxide nanoparticles using petals of Cassia glauca and evaluation of antimicrobial , enzyme inhibition , antioxidant , and nanozyme activities, Biochem. Syst. Ecol. 104 (104462) (2022) 1–9, https://doi.org/10.1016/j.bse.2022.104462.
[48] F.S. Sangsefidi, M. Nejati, J. Verdi, M. Salavati-Niasari, Green synthesis and characterization of cerium oxide nanostructures in the presence carbohydrate sugars as a capping agent and investigation of their cytotoxicity on the mesenchymal stem cell, J. Clean. Prod. 156 (2017) 741–749, https://doi.org/10.1016/j.jclepro.2017.04.114.
[49] D. Dutta, et al., Green synthesized cerium oxide nanoparticle: a prospective drug against oxidative harm, Colloids Surfaces B Biointerfaces 147 (2016) 45–53, https://doi.org/10.1016/j.colsurfb.2016.07.045.
[50] P. Maleki, F. Nemati, A. Gholoobi, A. Hashemzadeh, Z. Sabouri, M. Darroudi, Green facile synthesis of silver-doped cerium oxide nanoparticles and investigation of their cytotoxicity and antibacterial activity, Inorg. Chem. Commun. 131 (108762) (2021) 1–9, https://doi.org/10.1016/j.inoche.2021.108762.
[51] N. Hokonya, C. Mahamadi, N. Mukaratirwa-muchanyereyi, T. Gutu, C. Zvinowanda, Green synthesis of P - ZrO2CeO2ZnO nanoparticles using leaf extracts of Flacourtia indica and their application for the photocatalytic degradation of a model toxic dye, Congo red, 1–18, Heliyon 8 (2022) e10277, https://doi.org/10.1016/j.heliyon.2022.e10277.
[52] S. Sebastiammal, A. Mariappan, K. Neyvasagam, A. Lesly Fathima, Annona muricata inspired synthesis of CeO2 nanoparticles and their antimicrobial activity, Mater. Today Proc. 9 (2019) 627–632, https://doi.org/10.1016/j.matpr.2018.10.385.
[53] M. Fakhar-e-Alam, et al., Antitumor activity of zinc oxide nanoparticles fused with green extract of Nigella sativa, J. Saudi Chem. Soc. 28 (2) (2024) 1–6, https://doi.org/10.1016/j.jscs.2024.101814.
[54] D. Parimi, V. Sundararajan, O. Sadak, S. Gunasekaran, S.S. Mohideen, A. Sundaramurthy, Synthesis of positively and negatively charged CeO2 nanoparticles: investigation of the role of surface charge on growth and development of Drosophila melanogaster, ACS Omega 4 (1) (2019) 104–113, https://doi.org/10.1021/acsomega.8b02747.
[55] A. Umar, et al., An efficient chemical sensor based on CeO2 nanoparticles for the detection of acetylacetone chemical, J. Electroanal. Chem. 864 (114089) (2020) 1–8, https://doi.org/10.1016/j.jelechem.2020.114089.
[56] K. Rajesh, P. Sakthivel, A. Santhanam, J. Venugobal, Incorporation of silver ion on structural and optical characteristics of CeO2 nanoparticles: white LED applications, Optik 216 (164800) (2020) 1–10, https://doi.org/10.1016/j.ijleo.2020.164800.
[57] A. Krishnamoorthy, P. Sakthivel, I. Devadoss, V.M. Illayaraja Muthaiyaa, Structural, morphological and photoluminescence characteristics of Cd0.9-xZn0.1S quantum dots: effect of Fe2+ ion, Optik 205 (164220) (2020) 1–9, https://doi.org/10.1016/j.ijleo.2020.164220.
[58] V. Pisal, P. Wakchaure, N. Patil, S. Bhagwat, Green synthesized CeO2 quantum dots: a study of its antimicrobial potential, Mater. Res. Express 6 (11) (2019) 1–10, https://doi.org/10.1088/2053-1591/ab4fa5.
[59] R.P. Senthilkumar, V. Bhuvaneshwari, V. Malayaman, R. Ranjithkumar, S. Sathiyavimal, Phytochemical screening of aqueous leaf extract of Sida acuta burm. F. And its antibacterial activity, J. Emerg. Technol. Innov. Res. 5 (8) (2018) 474–478 [Online]. Available: www.jetir.org.
[60] S. Chandrasekaran, S. Anusuya, V. Anbazhagan, Anticancer, anti-diabetic, antimicrobial activity of zinc oxide nanoparticles: a comparative analysis, J. Mol. Struct. 1263 (133139) (2022) 1–12, https://doi.org/10.1016/j.molstruc.2022.133139.
[61] A.S. Fudala, W.M. Salih, F.F. Alkazaz, Synthesis different sizes of cerium oxide CeO2 nanoparticles by using different concentrations of precursor via sol–gel method, Mater. Today Proc. 49 (2021) 2786–2792, https://doi.org/10.1016/j.matpr.2021.09.452.
[62] R. Surega, B. Anita, S. Ramakrishnan, K. Gunasekaran, S. Nakkeran, Synthesis and characterization of AgNps using plant extracts 9 (2) (2020) 1939–1947.
[63] M.A. Taleb Safa, H. Koohestani, Green synthesis of silver nanoparticles with green tea extract from silver recycling of radiographic films, Results Eng 21 (2024) 1–6, https://doi.org/10.1016/j.rineng.2024.101808.
[64] A. Sathiyaseelan, K. Saravanakumar, M.-H. Wang, Cerium oxide decorated 5-fluorouracil loaded chitosan nanoparticles for treatment of hepatocellular carcinoma, Int. J. Biol. Macromol. 216 (June) (2022) 52–64, https://doi.org/10.1016/j.ijbiomac.2022.06.112.
[65] A. Bilal, J.K. Kasi, A.K. Kasi, M. Bokhari, S. Ahmed, S.W. Ali, Environment friendly synthesis of nickel ferrite nanoparticles using Brassica oleracea var . capitate (green cabbage) as a fuel and their structural and magnetic characterizations, Mater. Chem. Phys. 290 (126483) (2022) 1–10, https://doi.org/10.1016/j.matchemphys.2022.126483.
[66] S. Utara, S. Hunpratub, S. Pinitsoontorn, S. Phokha, Characterization and magnetic performance of pure CeO2 nanoparticles via an ozonolysis reaction, Results Phys. 30 (104890) (2021) 1–10, https://doi.org/10.1016/j.rinp.2021.104890.
[67] J. Eppakayala, M. Mettu, V.R. Pendyala, J.R. Madireddy, Synthesis , structural and optical properties of Ni doped ZnO nanoparticle – a chemical approach, Mater. Today Proc. 26 (2020) 148–153, https://doi.org/10.1016/j.matpr.2019.08.099.
[68] E. Barker, J. Shepherd, I.O. Asencio, The use of cerium compounds as antimicrobials for biomedical applications, Molecules 27 (9) (2022) 2678, https://doi.org/10.3390/molecules27092678.

[69] M. Zhang, C. Zhang, X. Zhai, F. Luo, Y. Du, C. Yan, Antibacterial mechanism and activity of cerium oxide nanoparticles, Sci. China Mater. 62 (11) (2019) 1–13, https://doi.org/10.1007/s40843-019-9471-7.
[70] L.S. Reddy Yadav, et al., Fruit juice extract mediated synthesis of CeO2 nanoparticles for antibacterial and photocatalytic activities, Eur. Phys. J. Plus 131 (5) (2016) 1–10, https://doi.org/10.1140/epjp/i2016-16154-y.
[71] Y. Dong, H. Zhu, Y. Shen, W. Zhang, L. Zhang, Antibacterial activity of silver nanoparticles of different particle size against Vibrio Natriegens, PLoS One 14 (9) (2019) 1–12, https://doi.org/10.1371/journal.pone.0222322.
[72] H. Yang, et al., Antibacterial effect of low-concentration ZnO nanoparticles on sulfate-reducing bacteria under visible light, Nanomaterials 13 (2023) 1–13, https://doi.org/10.3390/nano13142033.
[73] I.A.P. Farias, C.C.L. Dos Santos, F.C. Sampaio, Antimicrobial activity of cerium oxide nanoparticles on opportunistic microorganisms: a systematic review, BioMed Res. Int. 2018 (2018) 1–14, https://doi.org/10.1155/2018/1923606.
[74] G.X. Tong, et al., Polymorphous ZnO complex architectures: selective synthesis, mechanism, surface area and Zn-polar plane-codetermining antibacterial activity, J. Mater. Chem. B 1 (4) (2013) 454–463, https://doi.org/10.1039/c2tb00132b.
[75] P. Bellio et al., "Cerium oxide nanoparticles as potential antibiotic adjuvant. Effects of CeO 2 nanoparticles on bacterial outer membrane permeability," Biochim. Biophys. Acta - Biomembr., vol. xxx, no. xx, pp. xxx–xxx, doi: 10.1016/j.bbamem.2018.07.002.[.
[76] C. Kapadia, et al., Nanoparticles combined with cefixime as an effective synergistic strategy against Salmonella enterica typhi, Saudi J. Biol. Sci. 28 (8) (2021) 4164–4172, https://doi.org/10.1016/j.sjbs.2021.05.032.
[77] R. R. Patel Vidyasagar, S.K. Singh, D. Dehari, G. Nath, M. Singh, Facile green synthesis of silver nanoparticles derived from the medicinal plant Clerodendrum serratum and its biological activity against Mycobacterium species, 1–16, Heliyon 10 (10) (2024) e31116, https://doi.org/10.1016/j.heliyon.2024.e31116.
[78] O. Ayodele, E.O. Olanipekun, S.J. Olusegun, Synthesis, characterization, and antimicrobial evaluation of chitosan nanoparticles complexed with Ni(II) and Cu (II) ions, Bioresour. Technol. Reports 20 (2022) 1–6, https://doi.org/10.1016/j.biteb.2022.101218.